

Observation of $\pi^+\pi^-\pi^+\pi^-$ photoproduction in ultraperipheral heavy-ion collisions at $\sqrt{s_{NN}} = 200$ GeV at the STAR detector

B. I. Abelev,⁸ M. M. Aggarwal,³⁰ Z. Ahammed,⁴⁷ A. V. Alakhverdyants,¹⁷ B. D. Anderson,¹⁸ D. Arkhipkin,³ G. S. Averichev,¹⁷ J. Balewski,²² L. S. Barnby,² S. Baumgart,⁵² D. R. Beavis,³ R. Bellwied,⁵⁰ F. Benedosso,²⁷ M. J. Betancourt,²² R. R. Betts,⁸ A. Bhasin,¹⁶ A. K. Bhati,³⁰ H. Bichsel,⁴⁹ J. Bielcik,¹⁰ J. Bielcikova,¹¹ B. Biritz,⁶ L. C. Bland,³ B. E. Bonner,³⁶ J. Bouchet,¹⁸ E. Braidot,²⁷ A. V. Brandin,²⁵ A. Bridgeman,¹ E. Bruna,⁵² S. Bueltmann,²⁹ I. Bunzarov,¹⁷ T. P. Burton,² X. Z. Cai,⁴⁰ H. Caines,⁵² M. Calderón de la Barca Sánchez,⁵ O. Catu,⁵² D. Cebra,⁵ R. Cendejas,⁶ M. C. Cervantes,⁴² Z. Chajecski,²⁸ P. Chaloupka,¹¹ S. Chattopadhyay,⁴⁷ H. F. Chen,³⁸ J. H. Chen,⁴⁰ J. Y. Chen,⁵¹ J. Cheng,⁴⁴ M. Cherney,⁹ A. Chikanian,⁵² K. E. Choi,³⁴ W. Christie,³ P. Chung,¹¹ S. U. Chung,³ R. F. Clarke,⁴² M. J. M. Coddington,⁴² R. Corliss,²² J. G. Cramer,⁴⁹ H. J. Crawford,⁴ D. Das,⁵ S. Dash,¹³ A. Davila Leyva,⁴³ L. C. De Silva,⁵⁰ R. R. Debbé,³ T. G. Dedovich,¹⁷ M. DePhillips,³ A. A. Derevschikov,³² R. Derradi de Souza,⁷ L. Didenko,³ P. Djawotho,⁴² S. M. Dogra,¹⁶ X. Dong,²¹ J. L. Drachenberg,⁴² J. E. Draper,⁵ J. C. Dunlop,³ M. R. Dutta Mazumdar,⁴⁷ L. G. Efimov,¹⁷ E. Elhalhuli,² M. Elnimr,⁵⁰ J. Engelage,⁴ G. Eppley,³⁶ B. Erazmus,⁴¹ M. Estienne,⁴¹ L. Eun,³¹ O. Evdokimov,⁸ P. Fachini,³ R. Fatemi,¹⁹ J. Fedorisin,¹⁷ R. G. Fersch,¹⁹ P. Filip,¹⁷ E. Finch,⁵² V. Fine,³ Y. Fisyak,³ C. A. Gagliardi,⁴² D. R. Gangadharan,⁶ M. S. Ganti,⁴⁷ E. J. Garcia-Solis,⁸ A. Geromitsos,⁴¹ F. Geurts,³⁶ V. Ghazikhanian,⁶ P. Ghosh,⁴⁷ Y. N. Gorbunov,⁹ A. Gordon,³ O. Grebenyuk,²¹ D. Grosnick,⁴⁶ B. Grube,³⁴ S. M. Guertin,⁶ A. Gupta,¹⁶ N. Gupta,¹⁶ W. Guryon,³ B. Haag,⁵ T. J. Hallman,³ A. Hamed,⁴² L.-X. Han,⁴⁰ J. W. Harris,⁵² J. P. Hays-Wehle,²² M. Heinz,⁵² S. Heppelmann,³¹ A. Hirsch,³³ E. Hjort,²¹ A. M. Hoffman,²² G. W. Hoffmann,⁴³ D. J. Hofman,⁸ R. S. Hollis,⁸ H. Z. Huang,⁶ T. J. Humanic,²⁸ L. Huo,⁴² G. Igo,⁶ A. Iordanova,⁸ P. Jacobs,²¹ W. W. Jacobs,¹⁵ P. Jakl,¹¹ C. Jena,¹³ F. Jin,⁴⁰ C. L. Jones,²² P. G. Jones,² J. Joseph,¹⁸ E. G. Judd,⁴ S. Kabana,⁴¹ K. Kajimoto,⁴³ K. Kang,⁴⁴ J. Kapitan,¹¹ K. Kauder,⁸ D. Keane,¹⁸ A. Kechechyan,¹⁷ D. Kettler,⁴⁹ D. P. Kikola,²¹ J. Kiryluk,²¹ A. Kisiel,⁴⁸ S. R. Klein,²¹ A. G. Knospe,⁵² A. Kocoloski,²² D. D. Koetke,⁴⁶ T. Kollegger,¹² J. Konzer,³³ M. Kopytine,¹⁸ I. Koralt,²⁹ W. Korsch,¹⁹ L. Kotchenda,²⁵ V. Kouchpil,¹¹ P. Kravtsov,²⁵ K. Krueger,¹ M. Krus,¹⁰ L. Kumar,³⁰ P. Kurnadi,⁶ M. A. C. Lamont,³ J. M. Landgraf,³ S. LaPointe,⁵⁰ J. Lauret,³ A. Lebedev,³ R. Lednicky,¹⁷ C.-H. Lee,³⁴ J. H. Lee,³ W. Leight,²² M. J. LeVine,³ C. Li,³⁸ L. Li,⁴³ N. Li,⁵¹ W. Li,⁴⁰ X. Li,³³ X. Li,³⁹ Y. Li,⁴⁴ Z. Li,⁵¹ G. Lin,⁵² S. J. Lindenbaum,²⁶ M. A. Lisa,²⁸ F. Liu,⁵¹ H. Liu,⁵ J. Liu,³⁶ T. Ljubicic,³ W. J. Llope,³⁶ R. S. Longacre,³ W. A. Love,³ Y. Lu,³⁸ G. L. Ma,⁴⁰ Y. G. Ma,⁴⁰ D. P. Mahapatra,¹³ R. Majka,⁵² O. I. Mall,⁵ L. K. Mangotra,¹⁶ R. Manweiler,⁴⁶ S. Margetis,¹⁸ C. Markert,⁴³ H. Masui,²¹ H. S. Matis,²¹ Yu. A. Matulenko,³² D. McDonald,³⁶ T. S. McShane,⁹ A. Meschanin,³² R. Milner,²² N. G. Minaev,³² S. Mioduszewski,⁴² A. Mischke,²⁷ M. K. Mitrovski,¹² B. Mohanty,⁴⁷ M. M. Mondal,⁴⁷ D. A. Morozov,³² M. G. Munhoz,³⁷ B. K. Nandi,¹⁴ C. Nattaras,⁵² T. K. Nayak,⁴⁷ J. M. Nelson,² P. K. Netrakanti,³³ M. J. Ng,⁴ L. V. Nogach,³² S. B. Nurushev,³² G. Odyniec,²¹ A. Ogawa,³ H. Okada,³ V. Okorokov,²⁵ D. Olson,²¹ M. Pachr,¹⁰ B. S. Page,¹⁵ S. K. Pal,⁴⁷ Y. Pandit,¹⁸ Y. Panebratsev,¹⁷ T. Pawlak,⁴⁸ T. Peitzmann,²⁷ V. Perevozchikov,³ C. Perkins,⁴ W. Peryt,⁴⁸ S. C. Phatak,¹³ P. Pile,³ M. Planinic,⁵³ M. A. Ploskon,²¹ J. Pluta,⁴⁸ D. Plyku,²⁹ N. Poljak,⁵³ A. M. Poskanzer,²¹ B. V. K. S. Potukuchi,¹⁶ C. B. Powell,²¹ D. Prindle,⁴⁹ C. Pruneau,⁵⁰ N. K. Pruthi,³⁰ P. R. Pujahari,¹⁴ J. Putschke,⁵² R. Raniwala,³⁵ S. Raniwala,³⁵ R. L. Ray,⁴³ R. Redwine,²² R. Reed,⁵ J. M. Rehberg,¹² H. G. Ritter,²¹ J. B. Roberts,³⁶ O. V. Rogachevskiy,¹⁷ J. L. Romero,⁵ A. Rose,²¹ C. Roy,⁴¹ L. Ruan,³ M. J. Russcher,²⁷ R. Sahoo,⁴¹ S. Sakai,⁶ I. Sakrejda,²¹ T. Sakuma,²² S. Salur,⁵ J. Sandweiss,⁵² E. Sangaline,⁵ J. Schambach,⁴³ R. P. Scharenberg,³³ N. Schmitz,²³ T. R. Schuster,¹² J. Seele,²² J. Seger,⁹ I. Selyuzhenkov,¹⁵ P. Seyboth,²³ E. Shahaliev,¹⁷ M. Shao,³⁸ M. Sharma,⁵⁰ S. S. Shi,⁵¹ E. P. Sichtermann,²¹ F. Simon,²³ R. N. Singaraju,⁴⁷ M. J. Skoby,³³ N. Smirnov,⁵² P. Sorensen,³ J. Sowinski,¹⁵ H. M. Spinka,¹ B. Srivastava,³³ T. D. S. Stanislaus,⁴⁶ D. Staszak,⁶ J. R. Stevens,¹⁵ R. Stock,¹² M. Strikhanov,²⁵ B. Stringfellow,³³ A. A. P. Suaide,³⁷ M. C. Suarez,⁸ N. L. Subba,¹⁸ M. Sumbera,¹¹ X. M. Sun,²¹ Y. Sun,³⁸ Z. Sun,²⁰ B. Sorrow,²² T. J. M. Symons,²¹ A. Szanto de Toledo,³⁷ J. Takahashi,⁷ A. H. Tang,³ Z. Tang,³⁸ L. H. Tarini,⁵⁰ T. Tarnowsky,²⁴ D. Thein,⁴³ J. H. Thomas,²¹ J. Tian,⁴⁰ A. R. Timmins,⁵⁰ S. Timoshenko,²⁵ D. Tlusty,¹¹ M. Tokarev,¹⁷ T. A. Trainor,⁴⁹ V. N. Tram,²¹ S. Trentalange,⁶ R. E. Tribble,⁴² O. D. Tsai,⁶ J. Ulery,³³ T. Ullrich,³ D. G. Underwood,¹ G. Van Buren,³ G. van Nieuwenhuizen,²² J. A. Vanfossen Jr.,¹⁸ R. Varma,¹⁴ G. M. S. Vasconcelos,⁷ A. N. Vasiliev,³² F. Videbaek,³ Y. P. Vijoyi,⁴⁷ S. Vokal,¹⁷ S. A. Voloshin,⁵⁰ M. Wada,⁴³ M. Walker,²² F. Wang,³³ G. Wang,⁶ H. Wang,²⁴ J. S. Wang,²⁰ Q. Wang,³³ X. Wang,⁴⁴ X. L. Wang,³⁸ Y. Wang,⁴⁴ G. Webb,¹⁹ J. C. Webb,³ G. D. Westfall,²⁴ C. Whitten Jr.,⁶ H. Wieman,²¹ E. Wingfield,⁴³ S. W. Wissink,¹⁵ R. Witt,⁴⁵ Y. Wu,⁵¹ W. Xie,³³ N. Xu,²¹ Q. H. Xu,³⁹ W. Xu,⁶ Y. Xu,³⁸ Z. Xu,³ L. Xue,⁴⁰ Y. Yang,²⁰ P. Yepes,³⁶ K. Yip,³ I.-K. Yoo,³⁴ Q. Yue,⁴⁴ M. Zawisza,⁴⁸ H. Zbroszczyk,⁴⁸ W. Zhan,²⁰ S. Zhang,⁴⁰ W. M. Zhang,¹⁸ X. P. Zhang,²¹ Y. Zhang,²¹ Z. P. Zhang,³⁸ J. Zhao,⁴⁰ C. Zhong,⁴⁰ J. Zhou,³⁶ W. Zhou,³⁹ X. Zhu,⁴⁴ Y. H. Zhu,⁴⁰ R. Zoulkarneev,¹⁷ and Y. Zoulkarneeva¹⁷

(STAR Collaboration)

¹Argonne National Laboratory, Argonne, Illinois 60439, USA²University of Birmingham, Birmingham, United Kingdom³Brookhaven National Laboratory, Upton, New York 11973, USA⁴University of California, Berkeley, California 94720, USA⁵University of California, Davis, California 95616, USA⁶University of California, Los Angeles, California 90095, USA⁷Universidade Estadual de Campinas, Sao Paulo, Brazil

- ⁸University of Illinois at Chicago, Chicago, Illinois 60607, USA
⁹Creighton University, Omaha, Nebraska 68178, USA
¹⁰Czech Technical University in Prague, FNSPE, Prague, 115 19, Czech Republic
¹¹Nuclear Physics Institute AS CR, CZ-250 68 Řež/Prague, Czech Republic
¹²University of Frankfurt, Frankfurt, Germany
¹³Institute of Physics, Bhubaneswar 751005, India
¹⁴Indian Institute of Technology, Mumbai, India
¹⁵Indiana University, Bloomington, Indiana 47408, USA
¹⁶University of Jammu, Jammu 180001, India
¹⁷Joint Institute for Nuclear Research, Dubna, RU-141980, Russia
¹⁸Kent State University, Kent, Ohio 44242, USA
¹⁹University of Kentucky, Lexington, Kentucky, 40506-0055, USA
²⁰Institute of Modern Physics, Lanzhou, People's Republic of China
²¹Lawrence Berkeley National Laboratory, Berkeley, California 94720, USA
²²Massachusetts Institute of Technology, Cambridge, Massachusetts 02139-4307, USA
²³Max-Planck-Institut für Physik, Munich, Germany
²⁴Michigan State University, East Lansing, Michigan 48824, USA
²⁵Moscow Engineering Physics Institute, Moscow, Russia
²⁶City College of New York, New York, New York 10031, USA
²⁷NIKHEF and Utrecht University, Amsterdam, The Netherlands
²⁸Ohio State University, Columbus, Ohio 43210, USA
²⁹Old Dominion University, Norfolk, Virginia, 23529, USA
³⁰Panjab University, Chandigarh 160014, India
³¹Pennsylvania State University, University Park, Pennsylvania 16802, USA
³²Institute of High Energy Physics, Protvino, Russia
³³Purdue University, West Lafayette, Indiana 47907, USA
³⁴Pusan National University, Pusan, Republic of Korea
³⁵University of Rajasthan, Jaipur 302004, India
³⁶Rice University, Houston, Texas 77251, USA
³⁷Universidade de Sao Paulo, Sao Paulo, Brazil
³⁸University of Science & Technology of China, Hefei 230026, People's Republic of China
³⁹Shandong University, Jinan, Shandong 250100, People's Republic of China
⁴⁰Shanghai Institute of Applied Physics, Shanghai 201800, People's Republic of China
⁴¹SUBATECH, Nantes, France
⁴²Texas A&M University, College Station, Texas 77843, USA
⁴³University of Texas, Austin, Texas 78712, USA
⁴⁴Tsinghua University, Beijing 100084, People's Republic of China
⁴⁵United States Naval Academy, Annapolis, Maryland 21402, USA
⁴⁶Valparaiso University, Valparaiso, Indiana 46383, USA
⁴⁷Variable Energy Cyclotron Centre, Kolkata 700064, India
⁴⁸Warsaw University of Technology, Warsaw, Poland
⁴⁹University of Washington, Seattle, Washington 98195, USA
⁵⁰Wayne State University, Detroit, Michigan 48201, USA
⁵¹Institute of Particle Physics, CCNU (HZNU), Wuhan 430079, People's Republic of China
⁵²Yale University, New Haven, Connecticut 06520, USA
⁵³University of Zagreb, Zagreb, HR-10002, Croatia
- (Received 4 December 2009; published 2 April 2010)

We present a measurement of $\pi^+\pi^-\pi^+\pi^-$ photonuclear production in ultraperipheral Au-Au collisions at $\sqrt{s_{NN}} = 200$ GeV from the STAR experiment. The $\pi^+\pi^-\pi^+\pi^-$ final states are observed at low transverse momentum and are accompanied by mutual nuclear excitation of the beam particles. The strong enhancement of the production cross section at low transverse momentum is consistent with coherent photoproduction. The $\pi^+\pi^-\pi^+\pi^-$ invariant mass spectrum of the coherent events exhibits a broad peak around 1540 ± 40 MeV/ c^2 with a width of 570 ± 60 MeV/ c^2 , in agreement with the photoproduction data for the $\rho^0(1700)$. We do not observe a corresponding peak in the $\pi^+\pi^-$ final state and measure an upper limit for the ratio of the branching fractions of the $\rho^0(1700)$ to $\pi^+\pi^-$ and $\pi^+\pi^-\pi^+\pi^-$ of 2.5% at 90% confidence level. The ratio of $\rho^0(1700)$ and $\rho^0(770)$ coherent production cross sections is measured to be $13.4 \pm 0.8_{\text{stat.}} \pm 4.4_{\text{sys.}}\%$.

I. INTRODUCTION

The electromagnetic field of a relativistic heavy nucleus can be approximated by a flux of quasireal virtual photons using the Weizsäcker-Williams approach [1]. Because the number of photons grows with the square of the nuclear charge, fast-moving heavy ions generate intense photon fluxes. Relativistic heavy ions can thus be used as photon sources or targets. Because of the long range of the electromagnetic interactions, they can be separated from the hadronic interactions by requiring impact parameter b larger than the sum of the nuclear radii R_A of the beam particles. These so-called ultraperipheral heavy-ion collisions (UPCs) allow us to study photonuclear effects, as well as photon-photon interactions [2].

A typical high-energy photonuclear reaction in UPCs is the production of vector mesons. In this process, the virtual photon, radiated by the “emitter” nucleus, fluctuates into a virtual $q\bar{q}$ pair, which scatters elastically off the “target” nucleus, thus producing a real vector meson. The scattering can be described in terms of soft Pomeron exchange. The cross section for vector meson production depends on how the virtual $q\bar{q}$ pair couples to the target nucleus. This is determined mainly by the transverse momentum p_T of the produced meson. For small transverse momenta of the order of $p_T \lesssim \hbar/R_A$, the $q\bar{q}$ pair couples coherently to the entire nucleus. This leads to large cross sections that depend on the nuclear form factor $F(t)$, where t is the square of the momentum transfer to the target nucleus. For larger transverse momenta, the $q\bar{q}$ pair couples to the individual nucleons in the target nucleus. This “incoherent” scattering has a smaller cross section that scales approximately with the mass number A modulo corrections for nuclear absorption of the meson.

Because of the intense photon flux in UPCs, it is possible that vector meson production is accompanied by Coulomb excitation of the beam particles. The excited ions decay mostly via the emission of neutrons [3], which is a distinctive event signature that is utilized in the trigger decision. To lowest order, events with mutual nuclear dissociation are described by three-photon exchange (see Fig. 1): one photon to produce the vector meson and two photons to excite the nuclei. All three photon exchanges are in good approximation independent, so that the cross section for the production of a vector meson V accompanied by mutual nuclear dissociation can be factorized [3]:

$$\sigma_{V, xn, xn} = \int d^2b [1 - P_{\text{had}}(b)] P_V(b) P_{xn,1}(b) P_{xn,2}(b), \quad (1)$$

where $P_{\text{had}}(b)$ is the probability for hadronic interaction, $P_V(b)$ the probability of producing a vector meson V , and $P_{xn,i}(b)$ the probability that nucleus i emits x neutrons. Compared to exclusive photonuclear vector meson production, reactions with mutual Coulomb excitation have smaller median impact parameters.

The Particle Data Group (PDG) currently lists two excited ρ^0 states, the $\rho^0(1450)$ and the $\rho^0(1700)$, which are seen in various production modes and decay channels including

two- and four-pion final states [4]. The nature of these states is still an open question, because their decay patterns do not match quark model predictions [5]. Few data exist on high-energy photoproduction of excited ρ^0 states in the four-pion decay channel. Most of them are from photon-proton or photon-deuteron fixed-target experiments at photon energies in the range from 2.8 to 18 GeV [6–9]. The OMEGA spectrometer measured photoproduction on proton targets at energies E_γ of up to 70 GeV [10]. The heaviest target nucleus used so far to study diffractive two- and four-pion photoproduction was carbon with photon energies between 50 and 200 GeV [11]. These experiments observe a broad structure in the four-pion invariant mass distribution at masses ranging from 1430 ± 50 MeV/ c^2 [6] to 1570 ± 60 MeV/ c^2 [8] and with widths between 340 ± 60 MeV/ c^2 [8] and 850 ± 200 MeV/ c^2 [7] that the PDG assigns to the $\rho^0(1700)$. However, data indicate that the peak might consist of two resonances [9]. We will use the symbol ρ' to designate this structure in the rest of the text.

The measurements presented in this article extend the four-pion photoproduction data to fixed target equivalent photon energies of up to 320 GeV as well as to heavy target nuclei. This represents the first measurement of four-prong production in UPCs complementing the pioneering work on e^+e^- , $\rho^0(770)$, and J/ψ production in UPCs at STAR [12–15] and PHENIX [16].

There are at least three models for the production of $\rho^0(770)$ mesons in ultraperipheral collisions: The model of Klein and Nystrand (KN) [17] employs the vector dominance model (VDM) to describe the virtual photon and a classical mechanical approach for the scattering on the target nucleus, using results from $\gamma p \rightarrow \rho^0(770) p$ experiments. The Frankfurt, Strikman, and Zhalov (FSZ) model [18] is based on a generalized VDM for the virtual photon and a QCD Gribov-Glauber approach for the scattering. The model of Gonçalves and Machado (GM) [19] employs a QCD color dipole approach that takes into account nuclear effects and parton saturation phenomena. The KN model agrees best with the available data on $\rho^0(770)$ production; the FSZ and in particular the GM model overestimate the $\rho^0(770)$ production

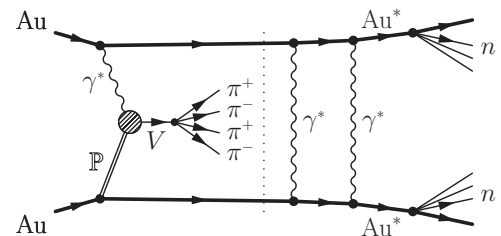


FIG. 1. Schematic view of the photonuclear production of a vector meson V in an ultraperipheral Au-Au collision and its subsequent decay into four charged pions. The meson production in the fusion processes of photon γ^* and Pomeron \mathbb{P} is accompanied by mutual Coulomb excitation of the beam ions. The processes are independent, as indicated by the dotted line.

cross section [14]. Only the FSZ calculations make predictions about the production of excited ρ^0 states in UPCs.

II. EXPERIMENTAL SETUP AND DATA SELECTION

The analysis is based on 1.9×10^6 events taken with the STAR experiment at the Relativistic Heavy Ion Collider (RHIC) in Au-Au collisions at $\sqrt{s_{NN}} = 200$ GeV during the year 2007 run. The Solenoidal Tracker at RHIC (STAR) experiment uses a large cylindrical time projection chamber (TPC) [20] with 2 m radius and 4.2 m length, operated in a 0.5-T solenoidal magnetic field, to reconstruct charged tracks.

Two detector systems are used for triggering: the central trigger barrel (CTB) [21], which is an array of 240 plastic scintillator slats around the TPC that allows us to trigger on charged particle multiplicities, and the two zero-degree calorimeters (ZDCs) [22], which are located ± 18 m from the interaction point. The ZDCs have an acceptance close to unity for neutrons originating from nuclear dissociation of the beam ions. In the trigger, these neutrons are used to tag UPC events by requiring coincident hits in both ZDCs with amplitudes corresponding to less than about seven to ten neutrons. The ADC sum of all CTB slats is restricted to a range equivalent to a hit multiplicity between about 2 and 40 minimum ionizing particles. To enrich events at central rapidities, events with hits above the minimum ionizing particle threshold in the large-tile beam-beam counters (BBCs) [23], which cover $2.1 < |\eta| < 3.6$, are vetoed.

In the offline analysis two- and four-prong data sets are selected. Four-prong events are required to have exactly four tracks with zero net charge in the TPC that form a common (primary) vertex. Because the STAR TPC has a drift time of about $36 \mu\text{s}$, any charged tracks produced within a time window of $\pm 36 \mu\text{s}$ around the triggered collision will overlap with the event of interest. Some of these additional tracks come from beam-induced background reactions, but, because of the high luminosities reached in the RHIC 2007 run [24], a large percentage is from real heavy-ion collisions. To account for those out-of-time events and backgrounds, up to 86 additional tracks per event, which do not point to the primary vertex, are allowed, but excluded from the analysis. The primary vertex is confined to a cylindrical region of 15 cm radius and 200 cm length centered around the interaction diamond, which reduces contaminations from pile-up events and beam-gas interactions. Each of the four-prong tracks is required to have at least 14 of a maximum possible 45 hits in the TPC. No particle identification is employed in the event selection; all four tracks are assumed to be pions. The distribution of the ionization energy loss dE/dx of the selected tracks in the TPC indicates that contaminations from other particle species are small. The transverse momentum distribution of the $\pi^+\pi^-\pi^+\pi^-$ combinations, as shown in Fig. 2, exhibits an enhancement at low p_T , characteristic of coherent production. Coherent events are selected by requiring $p_T < 150$ MeV/c. This cut also suppresses contaminations from peripheral hadronic interactions and from $\pi^+\pi^-\pi^+\pi^- + X$ events, where the X is not reconstructed.

Owing to charge conjugation invariance, we expect no $\rho^0(770)\rho^0(770)$ component in the diffractively produced

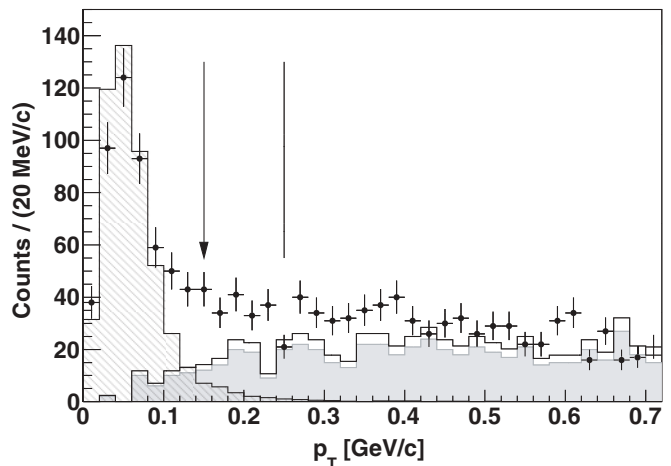


FIG. 2. Distribution of the $\pi^+\pi^-\pi^+\pi^-$ transverse momentum $p_T = |\sum_{i=1}^4 \vec{p}_{T,i}|$. The solid circles are the measured points with the statistical errors. The hatched histogram shows the expected distribution from simulation of coherent photoproduction (cf. Sec. III). The strong enhancement at low transverse momenta is attributable to coherently produced $\pi^+\pi^-\pi^+\pi^-$. This unique signature is used in the event selection, which requires $p_T < 150$ MeV/c (arrow). The remaining background is estimated from $+2-$ or -2 -charged four-prong combinations, by normalizing (factor = 1.186 ± 0.054) their p_T distribution (gray histogram) to that of the neutral four prongs in the region of $p_T > 250$ MeV/c (vertical line), yielding the open histogram (see section IV).

$\pi^+\pi^-\pi^+\pi^-$ final state. Possible contributions from $\rho^0(770)$ pair production by two independent photoproduction reactions on the same ion pair are negligible. The KN model predicts a cross-section ratio of exclusive photonuclear ρ^0 -pair production and exclusive single- ρ^0 production of about 1.2×10^{-3} [17]. For mutual nuclear dissociation of the beam ions, the ratio is expected to be of comparable value so that contaminations of the $\pi^+\pi^-\pi^+\pi^-$ sample by this process are at most a few percent. Also, $\gamma^*\gamma^* \rightarrow \rho^0(770)\rho^0(770)$ events contribute below the percent level. Here the cross-section ratio for exclusive ρ^0 -pair production in two-photon events and exclusive photonuclear $\rho^0(770)$ production was calculated to be 3.2×10^{-5} for $\rho^0(770)$ pair-invariant masses in the range between 1.5 and 1.6 GeV/c² [25].

The two-prong selection criteria are very similar and follow the STAR UPC $\rho^0(770)$ analyses [13,14]. As in the four-prong case, out-of-time events and background are taken into account by allowing up to 36 tracks per event in addition to the two primary TPC tracks. Background from two-photon e^+e^- and photonuclear ω production is negligible [14]. Cosmic-ray background is strongly suppressed, owing to the ZDC requirement in the trigger.

III. EFFICIENCY AND ACCEPTANCE CORRECTIONS

Detector efficiency and acceptance are studied using a Monte Carlo event generator based on the KN model [17], which describes coherent vector meson production accompanied by mutual Coulomb excitation in UPCs. To reduce

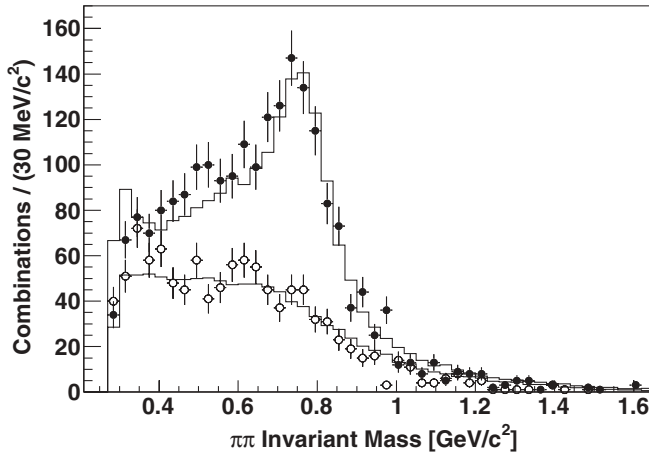


FIG. 3. Invariant mass distribution of two-pion subsystems. The solid circles show the measured $\pi^+\pi^-$ invariant mass spectrum for the selected four-prong sample (four entries per event) with statistical errors. The open circles represent the mass spectrum of the like-sign pion pairs (two entries per event). The unlike-sign mass distribution exhibits an enhancement with respect to the like-sign pairs in the $\rho^0(770)$ region. The histograms show the prediction from simulation assuming the relative S -wave decay $\rho' \rightarrow \rho^0(770) f_0(600)$.

model dependence, the acceptance corrections are applied in two stages. Within the detector acceptance of $|y| < 1$, the corrections are calculated using a realistic detector simulation based on GEANT 3 [26]. In a second step, the results are then extrapolated to the full 4π solid angle based on the KN model distributions.

To determine the acceptance corrections for the four-prong case, we assume a simple decay model, where an excited ρ^0 meson decays into $\rho^0(770)$ and $f_0(600)$, each in turn decaying into $\pi^+\pi^-$:

$$\rho' \rightarrow \rho^0(770) f_0(600) \rightarrow [\pi^+\pi^-]_{P \text{ wave}} [\pi^+\pi^-]_{S \text{ wave}}. \quad (2)$$

This decay model is motivated by the fact that the invariant mass spectrum of the unlike-sign two-pion subsystems in the four-prong sample shows an enhancement around the $\rho^0(770)$ mass (cf. Fig. 3). Figure 4 compares the invariant mass spectrum of the lightest $\pi^+\pi^-$ pair with the spectrum of the pair recoiling against it and shows that the four-pion final state consists mainly of a low-mass pion pair accompanied by a $\rho^0(770)$.

In principle, the ρ^0 and f_0 are allowed to be in a relative S or D wave, but, owing to the low statistics of the data, we are not able to estimate the D -wave parameters. Consequently, we consider only S -wave decay. Possible D -wave contributions are well within the estimated systematic error (see Sec. IV).

The angular distribution I that is used to estimate the acceptance corrections for the four-prong sample is parametrized as follows:

$$I \propto \sum_{\epsilon} \sum_{m, m'} \epsilon r_{m, m'} \epsilon \mathcal{A}_m^J \epsilon \mathcal{A}_{m'}^{J*}, \quad (3)$$

where \mathcal{A}_m^J is the amplitude for the decay of a ρ' with spin $J = 1$ and a projection m of J along the quantization axis

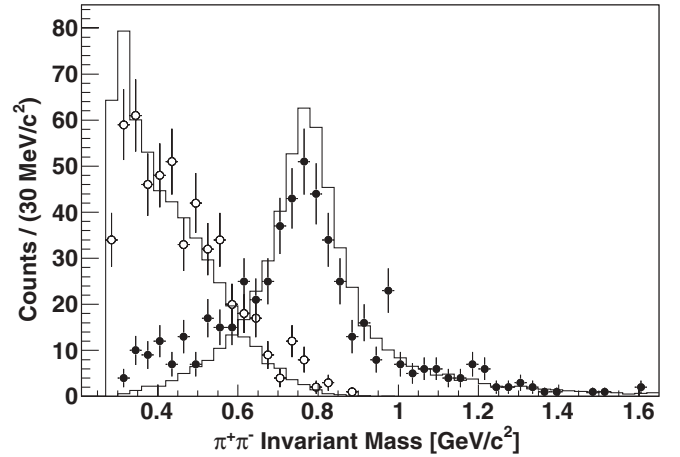


FIG. 4. Invariant mass distribution of two-pion subsystems. The open circles show the measured invariant mass spectrum of the lightest $\pi^+\pi^-$ pair in the event with the bars indicating the statistical errors. The filled circles represent the invariant mass distribution of the $\pi^+\pi^-$ that is recoiling against the lightest pair. The spectrum exhibits a clear peak in the $\rho^0(770)$ region. The histograms show the prediction from simulation assuming the relative S -wave decay $\rho' \rightarrow \rho^0(770) f_0(600)$.

assuming the model of Eq. (2). $\epsilon r_{m, m'}$ represents the spin-density-matrix elements. The amplitudes are defined in the ρ' rest frame with the z axis along the beam direction and the y axis parallel to the production plane normal, $\vec{p}_{\text{beam}} \times \vec{p}_{\rho'}$. Because of the large beam energy and the coherent nature of the production process, this frame coincides approximately with the ρ' helicity frame. Both the amplitudes and the spin-density matrix are constructed using eigenstates of the operator Π_y of reflections in the production plane, the so-called reflectivity basis with $\epsilon = \pm 1$ [27]. The sum in Eq. (3) is simplified by assuming s -channel helicity conservation (SCHC) and that the quasireal photons come with helicities ± 1 only, so that ${}^-r_{11} = {}^+r_{11}$ are the only nonzero spin-density-matrix elements. The amplitudes \mathcal{A}_m^J are factorized as follows:

$$\mathcal{A}_m^J = \Delta_{\rho}(m_{\rho}) \Delta_{f_0}(m_{f_0}) \epsilon \mathcal{M}_m^J(\theta, \phi; \theta_{\rho}, \phi_{\rho}, \gamma_{\rho}). \quad (4)$$

Here Δ_{ρ, f_0} are the amplitudes for the ρ^0 and f_0 resonance shapes as a function of the invariant masses of the intermediate states m_{ρ, f_0} . For the $\rho^0(770)$, a P -wave Breit-Wigner with mass-dependent width including Blatt-Weisskopf barrier factors is used [28]. The f_0 is modeled by an S -wave Breit-Wigner at 400 MeV/ c^2 with a width of 600 MeV/ c^2 . The decay amplitudes $\epsilon \mathcal{M}_m^J$ describe the angular dependence and include relativistic corrections via the Lorentz factor γ_{ρ} of the ρ^0 in the ρ' rest frame (RF) according to Ref. [29]. $\epsilon \mathcal{M}_m^J$ depends on the angles θ and ϕ of the ρ^0 in the ρ' rest frame, as well as on the angles θ_{ρ} and ϕ_{ρ} that describe the orientation of the π^+ from the ρ^0 decay in the ρ^0 helicity rest frame. This frame is defined starting from the ρ' rest frame and has its z_h axis parallel to the ρ^0 momentum and its y_h axis along the cross product of beam and ρ^0 momentum. Finally, the sums in Eq. (3) are Bose symmetrized to account for the four indistinguishable final-state configurations.

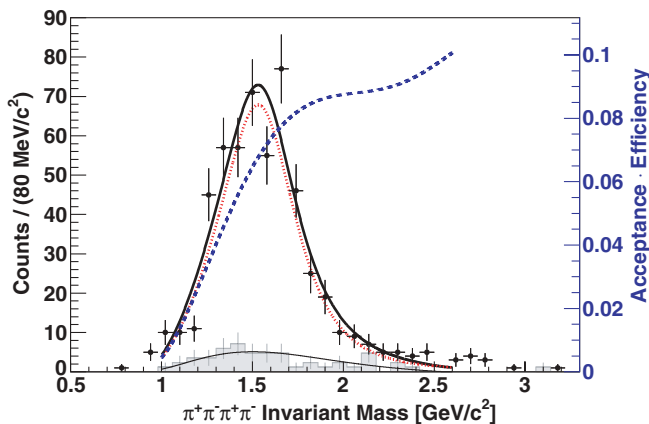


FIG. 5. (Color online) Invariant mass distribution of coherently produced $\pi^+\pi^-\pi^+\pi^-$. The filled circles are the measured points with the statistical errors, the gray histogram is the background estimated from charged four prongs (cf. Fig. 2). The thick black line shows the fit of a modified S -wave Breit-Wigner on top of a second-order polynomial background [thin black line; cf. Eq. (5)], taking into account the detector acceptance in the region $|y| < 1$ (rising dashed line). The dotted curve represents the signal curve without background.

The simulations agree well with the two- and four-pion kinematic distributions. The mean ρ^0 reconstruction efficiency in the region $|y| < 1$ is about $21.9 \pm 0.2\%$, that for the ρ' approximately $6.5 \pm 0.5\%$. The efficiencies show no strong dependence on the z position of the primary vertex or on the transverse momentum in the region of the coherent peak. However, owing to the TPC acceptance, the efficiencies decrease to roughly 1% for the ρ^0 and 0.1% for the ρ' , respectively, at $y = \pm 1$. The mass dependence of the ρ^0 efficiency is flat for masses above about $600 \text{ MeV}/c^2$ and decreases quickly for lower masses. The ρ' efficiency rises with mass, until it reaches a plateau at approximately $1500 \text{ MeV}/c^2$, so that the $\pi^+\pi^-\pi^+\pi^-$ mass peak in the uncorrected data is shifted toward larger masses (see the dashed curve in Fig. 5).

From the simulations the resolutions for p_T , y , and invariant mass of the selected pion pairs are estimated to be approximately $6 \text{ MeV}/c$, 0.009 , and $5 \text{ MeV}/c^2$, respectively. The corresponding values for the four-pion combinations are $10 \text{ MeV}/c$, 0.006 , and $10 \text{ MeV}/c^2$.

IV. RESULTS

The ratio of coherent ρ' and $\rho^0(770)$ production cross sections can be calculated from the respective acceptance-corrected yields, which are determined from fits of the $\pi^+\pi^-\pi^+\pi^-$ and $\pi^+\pi^-$ invariant mass distributions, respectively.

Figure 5 shows the measured $\pi^+\pi^-\pi^+\pi^-$ invariant mass spectrum, which exhibits a broad peak around $1540 \text{ MeV}/c^2$, indicating resonant ρ' production similar to what was seen in fixed-target photoproduction experiments [6–11]. This assumes that the peak is dominated by spin states with quantum numbers $J^{PC} = 1^{--}$. Contributions from other spin states

cannot be ruled out, because to disentangle them a much larger data set would be required.

The data are fit in the range from 1 to $2.6 \text{ GeV}/c^2$ with a relativistic S -wave Breit-Wigner that is modified by the phenomenological Ross-Stodolsky factor [30] and that sits on top of a second-order polynomial that parametrizes the remaining combinatorial background:

$$f_{4\pi}(m) = A \left(\frac{m_0}{m} \right)^n \frac{m_0^2 \Gamma_0^2}{(m_0^2 - m^2)^2 + m_0^2 \Gamma_0^2} + f_{\text{BG}}(m). \quad (5)$$

Here m is the $\pi^+\pi^-\pi^+\pi^-$ invariant mass. The resonance mass m_0 , the width Γ_0 , and the exponent n are left as free parameters.

The background polynomial f_{BG} is fixed by fitting the invariant mass distribution of $+2-$ or $-2-$ charged four prongs. Because at larger p_T the coherent cross section becomes negligible, the region $p_T > 250 \text{ MeV}/c$ is used to define the total amount of background by scaling the p_T distribution of the charged four prongs, so that it matches that of the neutral four prongs (cf. Fig. 2). This procedure treats incoherently produced $\pi^+\pi^-\pi^+\pi^-$ as background. The extracted scaling factor of 1.186 ± 0.054 —about half of the value estimated for the ρ^0 background (see later in this article)—is applied to the background polynomial.

Fitting Eq. (5) to the data yields a resonance mass of $1540 \pm 40 \text{ MeV}/c^2$, a width of $570 \pm 60 \text{ MeV}/c^2$, and an exponent of $n = 2.4 \pm 0.7$. The values for mass and width, however, depend strongly on the choice of n . The peak contains $N_{4\pi} = 9180 \pm 540$ events in the mass range from 1 to $2.6 \text{ GeV}/c^2$. As seen in Fig. 5 and also indicated by the χ^2 per degree of freedom of the maximum likelihood fit of about $36/16$, Eq. (5) does not describe the peak shape well. This is in accord with observations from other photoproduction experiments, which favor a description using two resonances in this mass region [9]. However, the low statistics of the data does not allow for the extraction of the resonance and mixing parameters for a two-resonance scenario.

In both the background and the signal fit, the mass dependence of the reconstruction efficiency for $|y| < 1$ is taken into account (dashed curve in Fig. 5). The efficiency is parametrized by a fifth-order polynomial determined by fitting the Monte Carlo data.

The $\rho^0(770)$ peak in the $\pi^+\pi^-$ invariant mass distribution of the selected two-prong data set is fit by a P -wave Breit-Wigner with mass-dependent width and Söding interference term [31] on top of a second-order polynomial background, as described in Refs. [13–15] (cf. Fig. 6). As in the ρ' case, the background polynomial is determined from a fit of the like-sign pair invariant mass distribution that is scaled up by a factor of 2.284 ± 0.050 , which is extracted from the incoherent part of the p_T distribution. The fit gives a ρ^0 mass of $772.3 \pm 1.2 \text{ MeV}/c^2$ and a width of $152.1 \pm 1.9 \text{ MeV}/c^2$, in agreement with both the PDG data on ρ^0 photoproduction [4] and earlier results from photonuclear production [13–15]. As expected, modifications of the $\rho^0(770)$ properties that were measured in peripheral Au-Au collisions [32] and attributed to in-medium production are not observed in the current study. The Breit-Wigner peak contains $N_\rho = 55\,940 \pm 910$ events in the mass

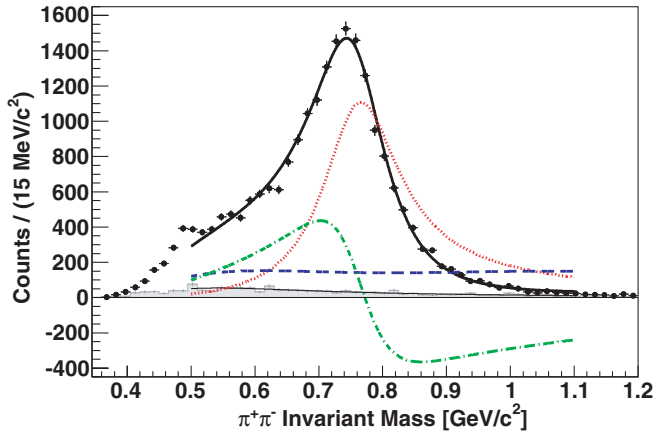


FIG. 6. (Color online) Invariant mass distribution of coherently produced $\pi^+\pi^-$ pairs. The solid circles are the measured points with statistical errors. The thick black line shows the fit taking into account the detector acceptance in the region $|y| < 1$. The noninterfering combinatorial background is represented by the thin black line, which is a fit to the like-sign invariant mass distribution scaled by a factor estimated from the p_T distribution (gray histogram). The dotted curve shows the Breit-Wigner without background; the dashed line shows the interfering background component that is assumed to be mass-independent. The dash-dotted curve is the Soding interference term of the two [31].

range from 500 to 1100 MeV/ c^2 . The χ^2 per degree of freedom of the maximum likelihood fit is 115/36, which mainly reflects the fact that the fit function does not reproduce well either the high mass tail of the $\rho(770)$ or the low-mass region. This mass region exhibits a peak from $K_s^0 \rightarrow \pi^+\pi^-$, where the kaons most likely come from photoproduced $\phi(1020)$.

Using the acceptance-corrected yields N_ρ and $N_{4\pi}$ for the $\rho^0(770)$ and the ρ' , respectively, it is possible to calculate the cross-section ratio for coherent ρ^0 and ρ' production, which is accompanied by mutual nuclear excitation and where the ρ' decays into $\pi^+\pi^-\pi^+\pi^-$:

$$\frac{\sigma_{4\pi, xn xn}^{\text{coh}}}{\sigma_{\rho, xn xn}^{\text{coh}}} = \frac{\sigma_{\rho', xn xn}^{\text{coh}} \mathcal{B}(\rho' \rightarrow \pi^+\pi^-\pi^+\pi^-)}{\sigma_{\rho, xn xn}^{\text{coh}}} = \frac{N_{4\pi}}{N_\rho}, \quad (6)$$

where $\mathcal{B}(\rho' \rightarrow \pi^+\pi^-\pi^+\pi^-)$ is the branching fraction of the ρ' into $\pi^+\pi^-\pi^+\pi^-$.

The cross-section ratio does not depend strongly on rapidity and in the region $|y| < 1$ has a mean value of $16.4 \pm 1.0_{\text{stat.}} \pm 5.2_{\text{syst.}}\%$. Based on the KN model [17] we estimate extrapolation factors to the full 4π solid angle of $1.8 \pm 0.1_{\text{syst.}}$ for the ρ' and of $2.2 \pm 0.1_{\text{syst.}}$ for the ρ^0 , where the latter value is taken from [14]. With this extrapolation, the overall coherent cross-section ratio is $13.4 \pm 0.8_{\text{stat.}} \pm 4.4_{\text{syst.}}\%$. Using the measured cross section $\sigma_{\rho, xn xn}^{\text{coh}}$ for coherent $\rho^0(770)$ production accompanied by mutual nuclear excitation of the beam particles from [14], the $\rho' \rightarrow \pi^+\pi^-\pi^+\pi^-$ production cross section can be calculated. The cross section within $|y| < 1$ is $\sigma_{4\pi, xn xn}^{\text{coh}}(|y| < 1) = 2.4 \pm 0.2_{\text{stat.}} \pm 0.8_{\text{syst.}}$ mb; the corresponding rapidity-integrated value is $\sigma_{4\pi, xn xn}^{\text{coh}} = 4.3 \pm 0.3_{\text{stat.}} \pm 1.5_{\text{syst.}}$ mb.

The influence of systematic effects on the cross-section ratio was studied. The main source of systematic uncertainty comes from the model dependence of the angular distribution of the $\pi^+\pi^-\pi^+\pi^-$ used in the acceptance correction. This uncertainty is estimated to be 21% by comparing to the cross-section ratio obtained using an isotropic angular distribution in the Monte Carlo simulation. The uncertainty from the parametrization of the $\pi^+\pi^-$ S wave in the four-prong-decay model is about 11% and is estimated by increasing the mass and/or width of the $f_0(600)$ Breit-Wigner to 600 and 1000 MeV/ c^2 , respectively. Additional systematic errors come from the event selection cuts (14%) and the background subtraction (10%), as well as the invariant mass binning and the fit range (8%). The systematic error associated with the particular choice of the fit function for the $\pi^+\pi^-\pi^+\pi^-$ invariant mass peak [cf. Eq. (5)] is estimated to be 9% by trying to fit a nonrelativistic Breit-Wigner and by fixing the value of the Ross-Stodolsky exponent in Eq. (5) to $n = 0$ and 4. The error for the extrapolation to the full 4π solid angle was estimated to be 6% for the ρ^0 in [14] by comparing the KN [17] and the FSZ [18] models. The extrapolation factor depends on the photon-energy spectrum, which is well known, and on the poorly known energy dependence of the photoproduction cross section. Because the KN model [17] describes the observed $\pi^+\pi^-\pi^+\pi^-$ rapidity distribution well, we assume that the ρ' production mechanism is not too different from that of the ρ^0 and assign the same systematic error of 6%.

The measured cross-section ratio cannot be compared directly to the ratio of the total exclusive coherent ρ' and ρ^0 cross sections of 14.2% predicted by the FSZ model [18], because the branching fraction for $\rho' \rightarrow \pi^+\pi^-\pi^+\pi^-$ is not known. The ratio between the cross section for ρ' production accompanied by mutual Coulomb excitation, as measured here, and the exclusive coherent ρ' cross section, where the beam ions remain unchanged, should be similar to the one for the ρ^0 . If in addition a 100% branching fraction to the $\pi^+\pi^-\pi^+\pi^-$ final state is assumed, the measured cross-section ratio agrees with the FSZ prediction. Under the same assumptions we can estimate, using the value for $\sigma_{\rho, 0n 0n}^{\text{coh}}$ from Ref. [14] and the measured cross-section ratio, the total exclusive coherent ρ' production cross section to be $\sigma_{\rho', 0n 0n}^{\text{coh}} = 53 \pm 4_{\text{stat.}} \pm 19_{\text{syst.}}$ mb. The value corresponding to the predicted cross-section ratio is $56 \pm 3_{\text{stat.}} \pm 8_{\text{syst.}}$ mb. These values are about half of the exclusive coherent ρ' cross section of 133 mb predicted by the FSZ model. However, this model predicts also ρ^0 cross-section values roughly twice larger than observed by experiment [14].

In previous photoproduction experiments using carbon targets, the ρ' was seen not only in the $\pi^+\pi^-\pi^+\pi^-$ decay mode, but also in $\pi^+\pi^-$ final states [11]. We do not observe a significant ρ' signal in the high-mass region of the $m_{\pi^+\pi^-}$ spectrum, as shown in Fig. 7. To suppress backgrounds, in particular cosmic rays, tighter cuts are applied: The rapidity is limited to $0.05 < |y| < 1$, the transverse momentum of the $\pi^+\pi^-$ pairs is required to be lower than 100 MeV/ c , and the primary vertex is confined to $|z_{\text{prim}}| < 70$ cm and $r_{\text{prim}} < 8$ cm.

The ρ' yield in the resulting $\pi^+\pi^-$ invariant mass spectrum is estimated by fitting the modified S -wave Breit-Wigner of Eq. (5) on top of an S -wave Breit-Wigner for the high-mass

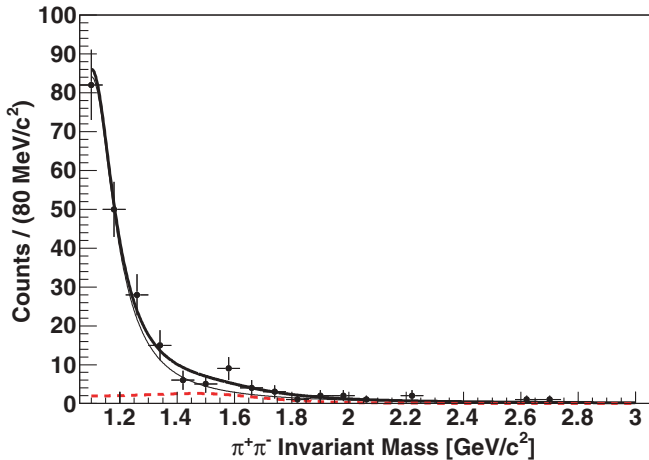


FIG. 7. (Color online) High-mass region of the $m_{\pi^+\pi^-}$ spectrum with tighter cuts applied to suppress background. The filled circles are the measured values with statistical errors. No significant enhancement is seen in the region around 1540 MeV/c², where the $\pi^+\pi^-\pi^+\pi^-$ invariant mass spectrum exhibits a peak. The thick solid line shows the fit of a modified S -wave Breit-Wigner [cf. Eq. (5)] with parameters fixed to the values extracted from the fit of the $\pi^+\pi^-\pi^+\pi^-$ invariant mass distribution on top of an S -wave Breit-Wigner that describes the tail of the $\rho^0(770)$ (thin solid line), taking into account the detector acceptance. The dashed curve represents the signal curve without the ρ^0 tail.

tail of the $\rho^0(770)$ in the mass range from 1.1 to 3 GeV/c². Assuming that the ρ' peak shape is the same in the $\pi^+\pi^-$ channel, we fixed mass, width, and exponent of the ρ' Breit-Wigner to the values obtained from the fit of the $\pi^+\pi^-\pi^+\pi^-$ invariant mass distribution. This gives an acceptance- and background-corrected ρ' yield of $N_{2\pi} = 110 \pm 90$ in the mass range from 1 to 2.6 GeV/c². $N_{2\pi}$ can be compared directly to the ρ' yield $N_{4\pi}$ in the $\pi^+\pi^-\pi^+\pi^-$ channel so that the ratio of the branching fractions of the ρ' to $\pi^+\pi^-$ and to $\pi^+\pi^-\pi^+\pi^-$ can be calculated:

$$R = \frac{\mathcal{B}(\rho' \rightarrow \pi^+\pi^-)}{\mathcal{B}(\rho' \rightarrow \pi^+\pi^-\pi^+\pi^-)} = \frac{N_{2\pi}}{N_{4\pi}}. \quad (7)$$

Owing to the low statistics, the measured value of $R = 0.012 \pm 0.010$ has a large uncertainty. The systematic error from neglecting the P -wave nature of the $\pi^+\pi^-$ decay by

using a mass-independent resonance width in Eq. (5) is within the range of the statistical error. The corresponding upper limit of the ratio is $R < 2.5\%$ at 90% confidence level. This is an indication that, in the process measured here, R is smaller than the ratio of the total ρ' cross sections in the two- and four-pion channel on a carbon target that was measured to be $6.6 \pm 3.4\%$ [11].

V. CONCLUSIONS

We have observed diffractive photonuclear production of $\pi^+\pi^-\pi^+\pi^-$ final states in ultraperipheral relativistic heavy-ion collisions accompanied by mutual Coulomb excitation of the beam particles. The $\pi^+\pi^-\pi^+\pi^-$ invariant mass peak exhibits a broad peak around 1540 MeV/c². Under the assumption that the peak is dominated by spin states with $J^{PC} = 1^{--}$, this is consistent with the existing photoproduction data currently assigned to the $\rho^0(1700)$ by the PDG. No corresponding enhancement in the $\pi^+\pi^-$ invariant mass spectrum is found. The ratio of the branching fractions of the excited ρ^0 state to $\pi^+\pi^-$ and $\pi^+\pi^-\pi^+\pi^-$ final states is smaller than 2.5% at 90% confidence level. The coherent ρ' production cross section is $13.4 \pm 0.8_{\text{stat.}} \pm 4.4_{\text{syst.}}\%$ of that of the $\rho^0(770)$ meson.

ACKNOWLEDGMENTS

We thank the RHIC Operations Group and RCF at BNL, the NERSC Center at LBNL, and the Open Science Grid consortium for providing resources and support. This work was supported in part by the Offices of NP and HEP within the US DOE Office of Science; the US NSF; the Sloan Foundation; the DFG cluster of excellence ‘‘Origin and Structure of the Universe’’; CNRS/IN2P3, STFC, and EPSRC of the United Kingdom; FAPESP CNPq of Brazil; Ministry of Education and Science of the Russian Federation; NNSFC, CAS, MoST, and MoE of China; GA and MSMT of the Czech Republic; FOM and NWO of the Netherlands; DAE, DST, and CSIR of India; the Polish Ministry of Science and Higher Education; Korean Research Foundation; Ministry of Science, Education, and Sports of the Republic of Croatia; and the Russian Ministry of Science and Technology and RosAtom of Russia.

- [1] C. F. von Weizsäcker, *Z. Phys.* **88**, 612 (1934); E. J. Williams, *Phys. Rev.* **45**, 729 (1934).
 [2] G. Baur, K. Hencken, D. Trautmann, S. Sadovsky, and Yu. Kharlov, *Phys. Rep.* **364**, 359 (2002); F. Krauss, M. Greiner, and G. Soff, *Prog. Part. Nucl. Phys.* **39**, 503 (1997); C. A. Bertulani, S. R. Klein, and J. Nystrand, *Annu. Rev. Nucl. Part. Sci.* **55**, 271 (2005); A. J. Baltz *et al.*, *Phys. Rep.* **458**, 1 (2008).
 [3] A. J. Baltz, S. R. Klein, and J. Nystrand, *Phys. Rev. Lett.* **89**, 012301 (2002); G. Baur, K. Hencken, A. Aste, D. Trautmann, and S. R. Klein, *Nucl. Phys. A* **729**, 787 (2003).

- [4] C. Amsler *et al.*, *Phys. Lett. B* **667**, 1 (2008).
 [5] T. Barnes, F. E. Close, P. R. Page, and E. S. Swanson, *Phys. Rev. D* **55**, 4157 (1997); F. E. Close and P. R. Page, *ibid.* **56**, 1584 (1997); A. Donnachie and Yu. S. Kalashnikova, *ibid.* **60**, 114011 (1999).
 [6] H. H. Bingham *et al.*, *Phys. Lett. B* **41**, 635 (1972).
 [7] P. Schacht, I. Derado, D. C. Fries, J. Park, and D. Yount, *Nucl. Phys. B* **81**, 205 (1974).
 [8] G. Alexander, O. Benary, J. Gandsman, D. Lissauer, A. Levy, Y. Oren, and L. M. Rosenstein, *Phys. Lett. B* **57**, 487 (1975).
 [9] D. P. Barber *et al.*, *Z. Phys. C* **4**, 169 (1980).

- [10] D. Aston *et al.*, *Nucl. Phys. B* **189**, 15 (1981); M. Atkinson *et al.*, *Z. Phys. C* **26**, 499 (1985).
- [11] M. S. Atiya *et al.*, *Phys. Rev. Lett.* **43**, 1691 (1979).
- [12] J. Adams *et al.*, *Phys. Rev. C* **70**, 031902(R) (2004).
- [13] C. Adler *et al.*, *Phys. Rev. Lett.* **89**, 272302 (2002).
- [14] B. I. Abelev *et al.*, *Phys. Rev. C* **77**, 034910 (2008).
- [15] B. I. Abelev *et al.*, *Phys. Rev. Lett.* **102**, 112301 (2009).
- [16] S. Afanasiev *et al.*, *Phys. Lett. B* **679**, 321 (2009); D. G. d'Enterria (PHENIX Collaboration), [arXiv:nucl-ex/0601001](https://arxiv.org/abs/nucl-ex/0601001).
- [17] S. R. Klein and J. Nystrand, *Phys. Rev. C* **60**, 014903 (1999).
- [18] L. Frankfurt, M. Strikman, and M. Zhalov, *Phys. Lett. B* **537**, 51 (2002); *Phys. Rev. C* **67**, 034901 (2003).
- [19] V. P. Gonçalves and M. V. T. Machado, *Eur. Phys. J. C* **40**, 519 (2005).
- [20] M. Anderson *et al.*, *Nucl. Instrum. Methods Phys. Res. Sect. A* **499**, 659 (2003); **499**, 679 (2003).
- [21] F. S. Bieser *et al.*, *Nucl. Instrum. Methods Phys. Res. Sect. A* **499**, 766 (2003).
- [22] C. Adler *et al.*, *Nucl. Instrum. Methods Phys. Res. Sect. A* **470**, 488 (2001).
- [23] J. Kiryluk, in Proceedings of 16th International Spin Physics Symposium (SPIN 2004), Trieste, Italy, Oct. 2004, http://dx.doi.org/10.1142/9789812701909_0152, [arXiv:hep-ex/0501072](https://arxiv.org/abs/hep-ex/0501072).
- [24] A. Drees *et al.*, in Proceedings of Particle Accelerator Conference (PAC 07), Albuquerque, NM, June 2007.
- [25] J. Nystrand and S. R. Klein, in *Proceedings of the Workshop on Photon Interactions and the Photon Structure*, September 1998 (CERN, Lund, Sweden), p. 263, [arXiv:nucl-ex/9811007](https://arxiv.org/abs/nucl-ex/9811007); M. Klusek, W. Schäfer, and A. Szczurek, *Phys. Lett. B* **674**, 92 (2009).
- [26] GEANT 3.21 Package, CERN Program Library W5013.
- [27] S. U. Chung and T. L. Trueman, *Phys. Rev. D* **11**, 633 (1975).
- [28] F. von Hippel and C. Quigg, *Phys. Rev. D* **5**, 624 (1972).
- [29] S. U. Chung and J. M. Friedrich, *Phys. Rev. D* **78**, 074027 (2008); S. U. Chung, *ibid.* **57**, 431 (1998); **56**, 4419 (1997); **48**, 1225 (1993); CERN Yellow Report No. 71-8, 1971.
- [30] M. Ross and L. Stodolsky, *Phys. Rev.* **149**, 1172 (1966).
- [31] P. Söding, *Phys. Lett.* **19**, 702 (1966); J. J. Sakurai, *Ann. Phys.* **11**, 1 (1960); T. H. Bauer *et al.*, *Rev. Mod. Phys.* **50**, 261 (1978).
- [32] J. Adams *et al.*, *Phys. Rev. Lett.* **92**, 092301 (2004).